Dyes and Pigments 169 (2019) 66–72

Contents lists available at ScienceDirect

Dyes and Pigments

journal homepage: www.elsevier.com/locate/dyepig

A comprehensive experimental study of five fundamental phenothiazine geometries increasing the diversity of the phenothiazine dye class for dye-sensitized solar cells

Audun Formo Buene[a], Anders Hagfeldt[b], Bård Helge Hoff[a,*]

[a] Department of Chemistry, Norwegian University of Science and Technology, Høgskoleringen 5, NO-7491, Trondheim, Norway
[b] Laboratory of Photomolecular Science, Institute of Chemical Sciences and Engineering, École Polytechnique Fédérale de Lausanne (EPFL), Chemin des Alambics, Station 6, CH-1015, Lausanne, Switzerland

ARTICLE INFO

Keywords:
Geometry study
Phenothiazine
Dye-sensitized solar cells
Auxiliary donor position
π-spacer

ABSTRACT

Phenothiazine is a versatile scaffold frequently used in both pharmaceutical and photovoltaic applications. Still, the structural diversity within the class of phenothiazine sensitizers for dye-sensitized solar cells is minute. Substituents are found in 3, 7 and 10-positions, often all three. In this work, we report the synthesis and evaluation of sensitizers illuminating five geometries for the phenothiazine dye class, of which three are novel geometries. Eleven sensitizers were prepared, investigating auxiliary donor contributions, effect of π-spacer and also the position of the anchoring group. We have established that the π-spacer has to be connected *para* to the 10*H* nitrogen atom of phenothiazine, the 3-position. Also, thiophene is a far superior π-spacer than phenyl, but we were unable to find any significant photovoltaic performance differences between the 3,7 and 3,8 geometries. A higher dye loading for the 3,8 geometry indicates there is hidden potential in this geometry which could be harvested by further optimization. The best device of the study was fabricated with **AFB-27** of the 3,8 geometry delivering a PCE of 5.88% (J_{SC} = 10.28 mA cm^{-2}, V_{OC} = 773 mV, FF = 0.75) under 1 sun AM 1.5G illumination.

1. Introduction

The need for increasing global power production has sparked the development of a number of new photovoltaic technologies. Dye-sensitized solar cells (DSSCs) are promising candidates allowing solar cells to be semi-transparent, flexible and of tunable color [1]. Under ambient light conditions, DSSCs have out-performed most other long established PV technologies [2]. Hot applications of DSSCs include building integration [3] and the powering of an increasing amount of devices in the internet of things (IoT) [2,4]. This development has to a large extent been supported by the introduction of new redox shuttles based on cobalt and copper complexes [5–9].

The dyes utilized in DSSCs have traditionally been metal-complexes, where N719, N3 and N749 also known as 'black dye' are most well known. Zinc porphyrins are also highly successful sensitizers with a metal-organic core [10]. In terms of efficiency, these metal-based complexes have achieved PCEs up to 13.0% [11]. Although the absorption properties of these dyes are excellent, the extinction coefficients are usually moderate and dye aggregation, synthesis and purification are common challenges. Thus, metal-free dyes have emerged as a viable alternative [12].

Improving the stability and efficiency of metal-free dyes is where the main efforts in this research area have been placed, and the current record for metal-free dyes is 14.3% [9]. Triarylamines, phenothiazines and polythiophenes are common dye scaffolds [13,14]. Phenothiazine, and its oxygen analog phenoxazine, were among the early metal-free dyes, and studies of π-spacers containing isomerizable double bonds have been conducted [15,16]. Furthermore, this class of sensitizers have shown very promising results in DSSCs with aqueous electrolytes, as demonstrated by Lin et al. [17] The phenothiazine dye scaffold has been the subject of two recent reviews [18,19], and as with any other class of dyes, the main challenge is improving the light harvesting properties.

Despite its popularity, the phenothiazine class of dyes is not particularly diverse. Most dye molecules follow the same design principle. The π-spacer and/or anchoring group and the aromatic auxiliary donor is always in 3- and 7-position on the phenothiazine scaffold. On the phenothiazine nitrogen atom there is either an alkyl chain or an aromatic ring bearing an alkoxy group. Phenothiazine is also sometimes used as a symmetrical donor, which could be termed the 10*H*-geometry

* Corresponding author.
E-mail address: bard.h.hoff@ntnu.no (B.H. Hoff).

https://doi.org/10.1016/j.dyepig.2019.05.007
Received 29 March 2019; Received in revised form 26 April 2019; Accepted 3 May 2019
Available online 06 May 2019

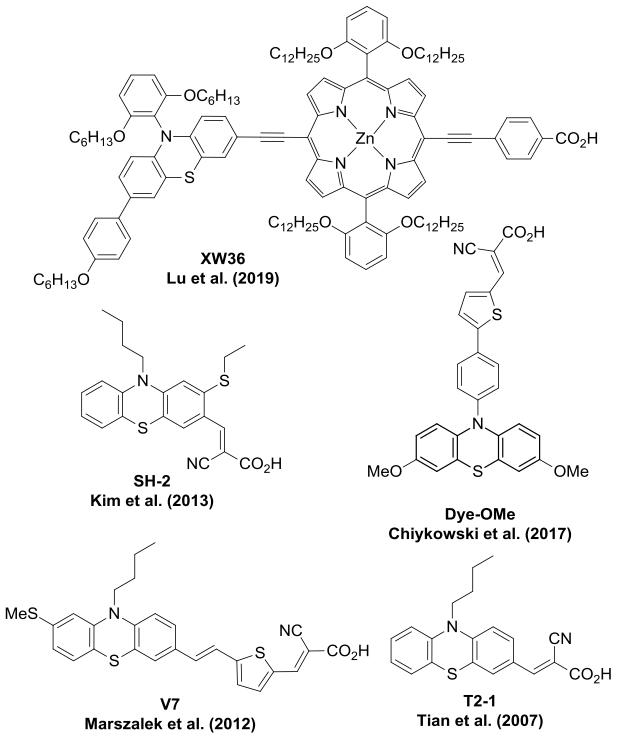

Fig. 1. A selection of reported phenothiazine sensitizers. The auxiliary donor of **XW36** [25] is an example of a 3,7-substiuted phenothiazine, **SH-2** [30] uses an ethylthio substituent in 2-position, **Dye-OMe** [24] has a 10*H*-geometry, dye **V7** (and the simpler **V5**) [29] is the only example of a phenothiazine sensitizer with a 3,8-geometry, while **T2-1**[15] is the very first phenothiazine sensitizer for DSSCs and has the common 3-geometry.

where the anchoring group is connected to the phenothiazine through the 10*H* nitrogen atom [20–24]. In this geometry, the phenothiazine is used as a locked diphenylamine substituent, and has been compared to analogous triphenylamine sensitizers and found less efficient in DSSCs [23]. Phenothiazine has also been used as an auxiliary donor on other metal-based sensitizers, such as zinc porphyrins [25–28].

Of the 246 phenothiazine sensitizers published in the 113 publications (as of 20th February 2019 on SciFinder) containing the concepts *phenothiazine* and *dye-sensitized solar cell*, only two publications report structures with different geometries. These examples and other phenothiazine-based dyes are shown in Fig. 1. Marszalek et al. published two dyes with a methylthio substituent in the 8-position on the phenothiazine scaffold, with the π-spacer in the 3-position (using the numbering established in this work) [29]. However, neither the donating effect nor the position of the methylthio substituent were investigated. The other example is published by Kim et al. investigating the effect of ethylthio substitution in 2-position with the anchoring group in 3-position [30]. The ethylthio substituent increased the molar J_{SC} values (mA/mol dye), but lower dye loading values limited the efficiency and no improvement in PCE was reported.

We have synthesized and evaluated a selection of simple dyes (see Fig. 2) intending to extend the geometry landscape of the phenothiazine dye class. By doing so we hope to shed some light on how the substitution geometry affects the photophysical, electrochemical and photovoltaic performance of phenothiazine sensitizers.

2. Results and discussion

2.1. Dye synthesis

In order to achieve large variation in substitution patterns for phenothiazine dyes, a number of synthetic routes had to be used. To improve the readability of this work we have constructed a new nomenclature system for the different geometries of phenothiazine sensitizers, naming the position of the π-spacer/anchoring group first with the lowest number, then the position of the auxiliary donor, separated by a comma, so **AFB-27** has the 3,8-geometry. If there is no auxiliary donor, the name of the geometry is dictated by the position of the π-spacer/anchoring group only, which is the case for **AFB-20**, which has a 3-geometry.

Routes to the standard 3,7 sensitizer geometry are frequently utilized in the field, also by our group in previous publications [31,32]. Sensitizers **AFB-20** and **22** were prepared along the same route, rather than through a monobromination approach. The excess bromine substituent was removed in a palladium catalyzed dehalogenation, based on a protocol reported by Chen et al. [33], as shown in Scheme 1 (ii). Sensitizer **AFB-20** has previously been synthesized and characterized a number of times [32,34,35].

For the simple dyes **AFB-23** and **24** with the π-spacer in 2-position, a very convenient route starting from 2-chloro-10*H*-phenothiazine was employed, see Scheme 1 (iii). Alkylation installed the hexyl chain and a Suzuki coupling introduced the aldehyde functionalized π-spacer precursor from commercial boronic acids. In our hands, the Suzuki coupling with 5-formyl-2-thienylboronic acid is sometimes a very poor reaction, especially when an aryl chloride is the coupling partner. Three equivalents of boronic acid were used, yet full conversion was still difficult to achieve, resulting in unimpressive yields for these reactions. The very reliable Knoevenagel condensation introducing the anchoring group was the last step for all the synthetic routes.

The dyes with 3,8 and 2,7 geometries were synthesized from the highly versatile building block **3**. Preparation of **3** was achieved through a bromination of 2-chloro-10*H*-phenothiazine by molecular bromine followed by alkylation with NaH and 1-bromohexane, see Scheme 1 (i). The challenge in this route was the highly non-selective bromination step. The resulting crude mixture initially contained approximately 50% of the desired compound **2** measured by ^{1}H NMR, and reached a purity of over 97% following three to five recrystallizations from toluene. Although tedious, this was possible on a large scale, and a reliable alkylation of **2** gave adequate amounts of building block **3** for further reactions. By using the building blocks **1** and **3**, in addition to 3,7-dibromo-10*H*-phenothiazine, all the sensitizers were synthesized successfully, and detailed procedures can be found in the ESI.

2.2. Photophysical properties

UV–Visible absorption spectra of all the sensitizers were recorded in THF and adsorbed on TiO_2 films. The solution spectra are shown in Fig. 3 and the TiO_2 film spectra in Fig. S4, while the extracted data are given in Table 1.

From such a diverse set of sensitizers, a number of different comparisons can be drawn from the UV/Vis data, as highlighted in Fig. S5 (a-d). With regards to the position of the π-spacer, the ICT transition peak of the sensitizers with the π-spacer in 3-position are both hyper- and bathocromically shifted compared to the 2-position. In general, there is a clear difference between the thiophene and phenyl π-spacers, with the absorption of the thiophene-based compounds being redshifted by approximately 40 nm. In Fig. S5 (b) hardly any differences can be found between the two positions of the auxiliary donors, i.e. the 3,7 and 3,8 geometries have very similar absorption spectra. And lastly, the position of the anchoring group on a phenyl π-spacer is very important, as positioning of the cyanoacrylic anchoring group in the *meta*-position is totally detrimental to the ICT transition of the sensitizer.

2.3. Electrochemical properties

Cyclic voltammetry on stained FTO/TiO_2 electrodes was performed in acetonitrile with 0.1 M LiTFSI as a supporting electrolyte, a graphite carbon rod as counter electrode and a Ag/AgCl reference electrode. The

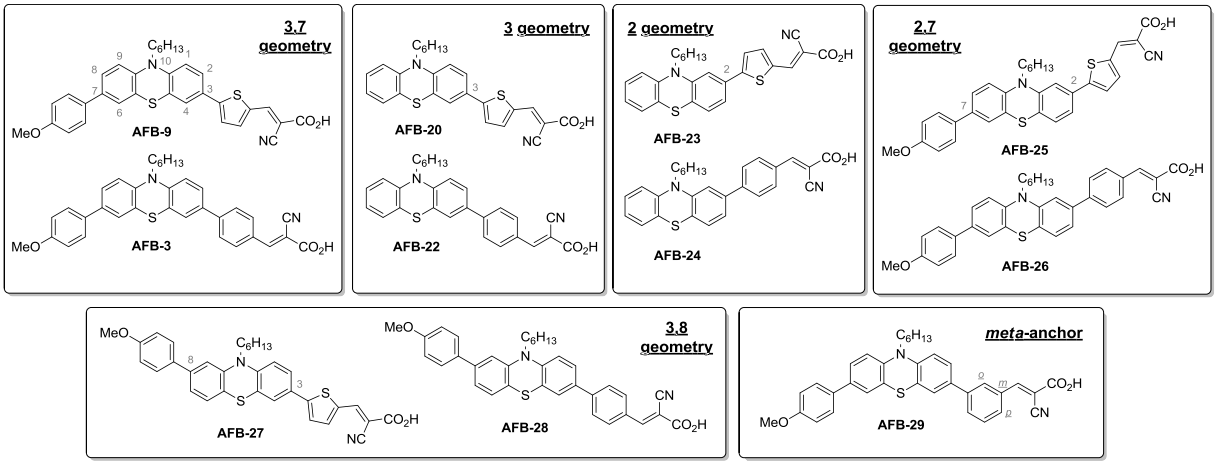

Fig. 2. Molecular structures of the sensitizers investigated in this study. The general numbering of the phenothiazine scaffold is shown for **AFB-9**.

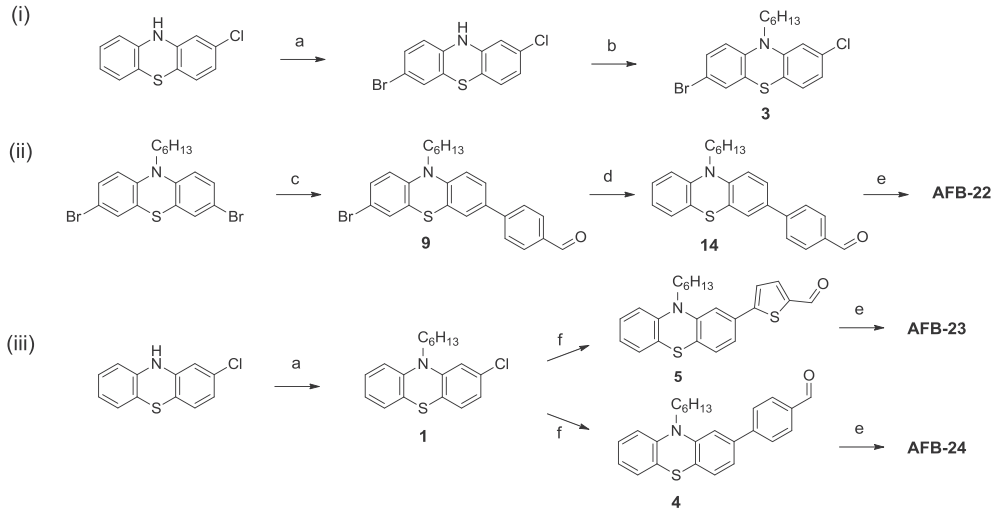

Scheme 1. Synthesis scheme to dyes **AFB-23**, **24** and **25**. a) Br_2, AcOH, b) NaH, 1-bromohexane, THF, c) boronic acid, $Pd(PPh_3)_4$, K_2CO_3, 1,4-dioxane/H_2O (1:1), d) $Pd(OAc)_2$, PPh_3, K_2CO_3, *n*-butanol, e) cyanoacetic acid, piperidine, CH_3CN, f) boronic acid, $Pd(OAc)_2$, SPhos, K_2CO_3, 1,4-dioxane/H_2O (1:1).

cyclic voltammograms are plotted in Fig. S6. All the sensitizers showed a single reversible oxidation in the range of 0.58–0.68 V vs. Ag/AgCl, while the $E_{1/2}$ value of ferrocene was found at 0.219 V vs. Ag/AgCl. Using the obtained sensitizer oxidation potentials and the optical bandgaps, the LUMO levels can be calculated, and the complete map of the HOMO-LUMO positions is given in Fig. 4. Sufficient potential differences are found for all dyes to have an efficient electron injection and be successfully regenerated from the I^-/I_3^- redox shuttle.

The HOMO levels are comparable for all the dyes, which is to be expected as they all share the same phenothiazine scaffold. A slight shift of the HOMO levels of 20–70 mV towards more negative potentials is observed when introducing the auxiliary donor, and the oxidation potentials of the thiophene-linked dyes are on average found 30 mV below (more positive potentials) their phenyl analogs. For the LUMO level position, the largest differences can be seen when comparing the dyes with thiophene and phenyl π-spacers, where the LUMO levels of the thiophene-linked dyes are found shifted at least 200 mV towards more positive potentials compared to the phenyl analogs. The *meta*-position of the anchoring group in **AFB-29** shifted the LUMO level up by almost 400 mV compared to the corresponding *para* derivative **AFB-3**, massively increasing the bandgap and lowering the light harvesting abilities considerably.

2.4. Photovoltaic properties

The AFB dyes of different geometry were utilized in DSSCs, and Fig. 5 (a and b) shows the current density-voltage curves under 1 sun AM 1.5G illumination of the best device fabricated for each sensitizer (average data presented in Table 2). The solar cells were fabricated from photoanodes with 16.5 µm TiO_2 (11 µm 18NR-T and 5.5 µm WER2-O scattering layer), platinum counter electrodes and an I^-/I_3^- electrolyte in a sandwich construction.

There are large differences in photovoltaic performance between the different geometries. The most efficient sensitizers were the thiophene containing **AFB-9** (3,7) and **AFB-27** (3,8) with incredibly similar average PCE values of 5.82% and 5.78%, respectively. For their phenyl analogs a small performance difference of 6% was found, in favor of the 3,8-geometry. Of the five different main geometries investigated in this work the order of photovoltaic performance was: 2 < 2,7 < 3 < 3,7 ≈ 3,8. The sensitizer delivering the lowest efficiency was not surprisingly **AFB-29**, confirming that the anchoring group position on a phenyl π-spacer has to be in the *para*-position. Thiophene was the most efficient π-spacer across all geometries, outperforming phenyl by an average of 33%, despite lower average V_{OC} values by 25 mV compared to the phenyl sensitizers. The 3,8-geometry was the least affected by the π-spacers with a performance difference of only 24% while the 2-geometry was most affected at 53% performance difference, also in favor of thiophene.

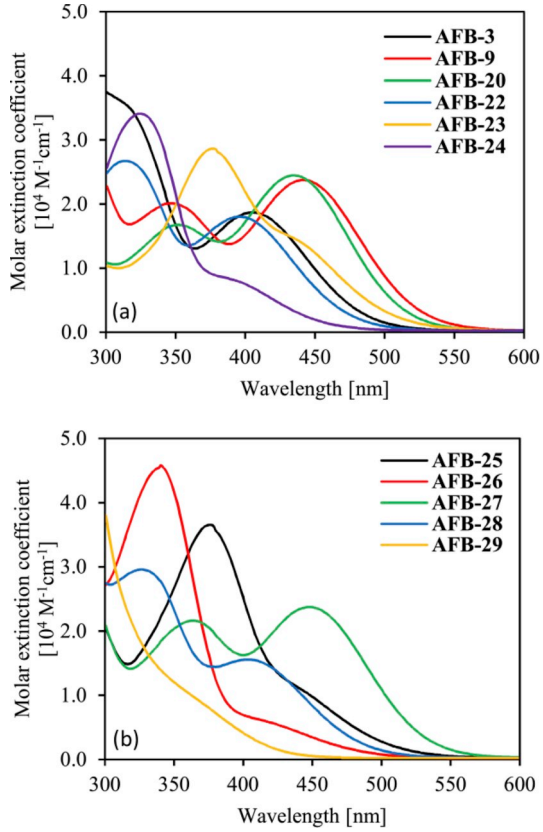

Fig. 3. UV–Visible spectra in THF solution (2×10^{-5} M).

The introduction of the 4-methoxyphenyl auxiliary donor separating the 3 from the 3,7 and 3,8 geometries improved the photovoltaic performance by 8–15%, supporting our previous findings on auxiliary donors for phenothiazine sensitizers [32]. However, the effect was considerably larger between the 2 and 2,7 geometries where the auxiliary donor improved the PCE by 37% on average.

In the IPCE spectra shown in Fig. 5 (c and d), the absorption onsets are redshifted by over 100 nm compared to the UV/Vis solution spectra recorded in THF, indicating the molecular environment is quite different inside the devices compared to in THF solution. For further studies, choosing a different solvent for UV/Vis analyses could yield spectra more closely matching the absorption properties in devices. The integrated short-circuit current densities from the IPCE spectra given in Table 2 are in reasonable agreement with the experimental J_{SC} values from the *J-V* sweeps, underestimating the J_{SC} by a maximum of 8%, requiring no further explanation. The highest IPCE values from the devices were just exceeding 70%, meaning there is potential for further device optimization to reach the maximum theoretical value, dictated by the transmittance of the FTO glass (normally in the range of 80–85% depending on sheet resistance).

Charge extraction and electron lifetime measurements were conducted on the best device from each sensitizer, presented in Fig. 6. From the charge extraction measurements, a relative conduction band shift of up to 72 mV is observed as the horizontal distance between the parallel charge extraction curves in Fig. 6 (a and b). This shift is explained as a change in the conduction band edge (E_{CB}) due to the protons released upon dye adsorption to TiO_2 [36]. This means dye loading, but also the pK_a of the sensitizers could affect the conduction band position. Electron lifetime measurements (see Fig. 6c, uncorrected measurements in Fig. S7 in the ESI) were obtained and processed following the same procedure described by the authors previously [32]. A separated grouping of the thiophene and phenyl π-spacer series is found, with higher electron lifetime values obtained for the sensitizers with phenyl spacers. This corresponds well to the observations from the *J-V* data, that these dyes have a 25 mV higher average V_{OC}, as the position of the Fermi level of TiO_2 depends on the conduction band position, the electron density and the injected electron lifetime. The higher lifetime values of the phenyl sensitizers indicates electron recombination is slower, and similar results have been reported previously [37]. There are two possible recombination pathways for the injected electrons in the TiO_2: (i) back to the dye cation, or (ii) to the oxidized redox shuttle species (either I_3^- or I_2). The recombination to the dye cation is usually reported to be a significantly slower process than (ii) [38], thus the effect observed here must be related to how the π-spacers restrict or promote access for the electrolyte through the dye monolayer to the TiO_2 surface [36]. The complexation between thiophene units and iodide anions has been proposed, a mechanism which could bring these species closer to the TiO_2 surface and hence accelerate this recombination pathway [39,40]. Despite the lower electron lifetimes, the thiophene π-spacers widen the absorption and improves the efficiency.

When comparing the phenyl sensitizers **AFB-3** (3,7) to **AFB-28** (3,8) and the thiophene derivatives **AFB-9** (3,7) to **AFB-27** (3,8), we observe closely grouped lifetime curves for both the 3,7 and 3,8 geometries, indicating that the position of the auxiliary donor does not affect the rate of recombination significantly.

From our investigations into the different geometries here reported,

Table 1
Photophysical properties of dyes **AFB-3, 9, 20, 22** to **29**.

Dye	Geo-metry	π-spacer	λ_{abs}[a] (nm)	ε ($M^{-1}cm^{-1}$)	Em.[b] (nm)	λ_{abs}[c] on TiO_2 (nm)	$E_{0\text{-}0}$[d] (eV)	E_{ox}[e] (V)	E_{LUMO}[f] (V)
AFB-3	3,7-*p*	Ph	406	18500	614	409	2.51	1.00	−1.51
AFB-9	3,7	Thio	442	23600	634	442	2.31	1.01	−1.30
AFB-20	3	Thio	435	24400	618	430	2.38	1.08	−1.30
AFB-22	3	Ph	396	17900	596	394	2.56	1.04	−1.52
AFB-23	2	Thio	433[g]	14700	639	–	2.36	1.07	−1.29
AFB-24	2	Ph	393[g]	7800	609	–	2.57	1.03	−1.54
AFB-25	2,7	Thio	442[g]	10800	649	–	2.32	1.05	−1.27
AFB-26	2,7	Ph	419[g]	5600	611	–	2.48	1.01	−1.47
AFB-27	3,8	Thio	449	23600	629	437	2.32	1.04	−1.28
AFB-28	3,8	Ph	404	15400	590	–	2.54	1.02	-1–52
AFB-29	3,7-*m*	Ph	358[g]	13400	471	–	2.85	0.98	−1.87

[a] Maximum of most red-shifted peak.
[b] Emission when ICT band is excited, in THF solution.
[c] Maximum of most red-shifted peak on TiO_2 (2.5 μm, GreatcellSolar 18NR-T).
[d] Calculated from the intersection of the absorption and normalized emission spectra.
[e] Measured vs. F_c^+/F_c on stained TiO_2 electrodes in acetonitrile with 0.1 M LiTFSI, converted to V vs. SHE by 0.624 V. Scan rate 20 mV s^{-1}.
[f] Calculated from E_{ox}-$E_{0\text{-}0}$.
[g] Manual estimate due to no clear peak to assign.

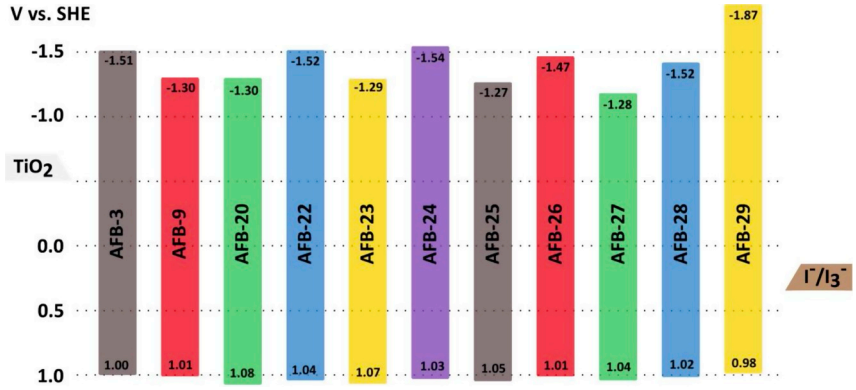

Fig. 4. Energy level diagram of the sensitizers.

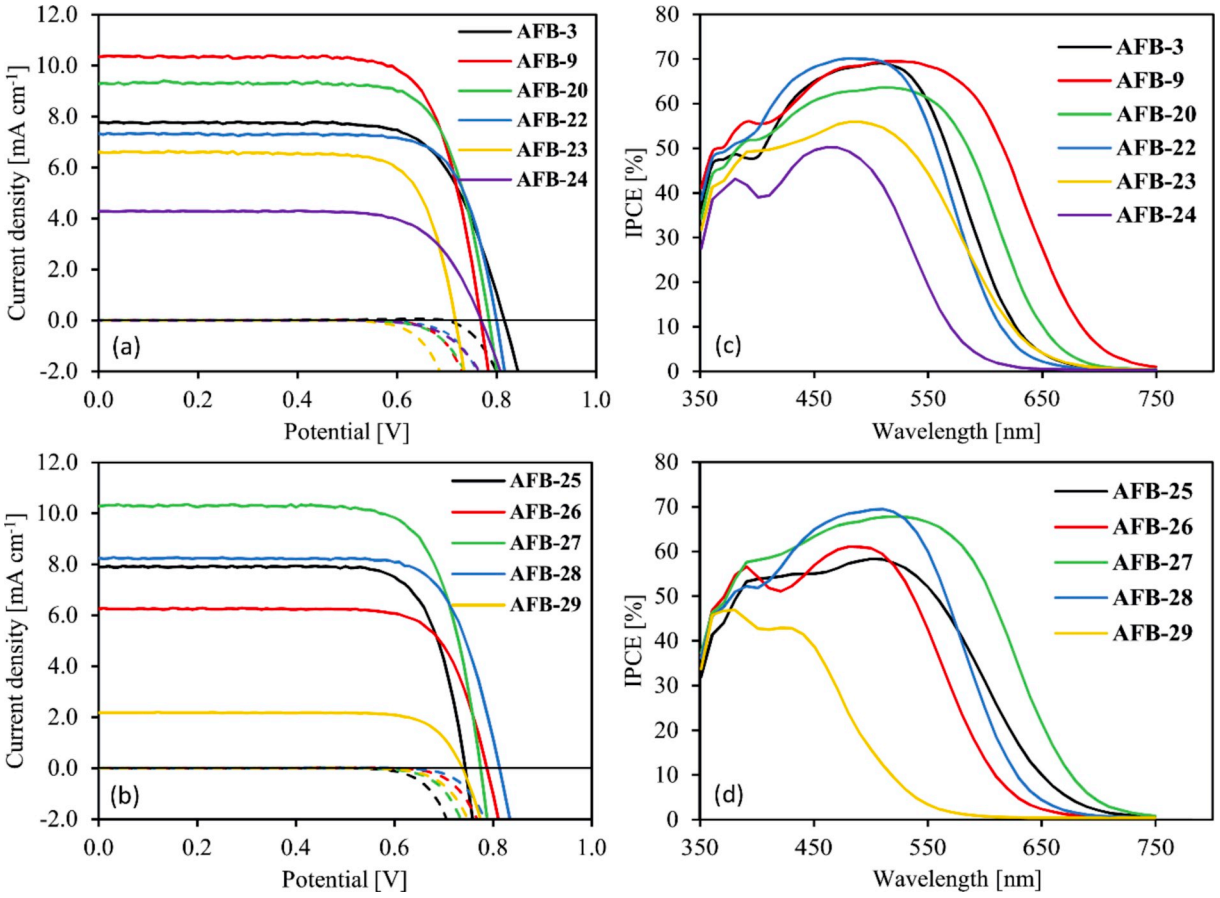

Fig. 5. (a–b) *J-V* curves for the best device for each sensitizer. Dashed lines are the dark current measurements. (c–d) IPCE spectra of the best device for each sensitizer.

we have a number of encouraging observations. Firstly, we were able to reproduce our previous findings of the modest positive effect from the auxiliary donors on phenothiazine sensitizers, improving the photovoltaic performance by around 10% [32]. Because the contribution from the auxiliary donor is only modest, we were unable to identify any effects from the position of this moiety. However, as we suspected the more linear 3,8 geometry to anchor on TiO_2 in a more perpendicular fashion, we did dye loading measurements with the pure sensitizers having thiophene as π-spacer **AFB-9** (3,7) and **AFB-27** (3,8) without the additive CDCA, see Table 3. Indeed, the 3,8 geometry displayed 10% higher dye loading, indicating there could be a performance advantage to the 3,8 geometry. This can also be seen from the electron lifetime measurements, where **AFB-27** has marginally higher electron lifetimes, suggesting a denser dye monolayer compared to **AFB-9**. We think the key to fully exploit this potential lies in optimizing the CDCA concentration in the staining solutions. Also, by increasing the size of the auxiliary donor, we believe any differences will be more pronounced.

Further, attachment of the π-spacer in the 3-position is vastly superior to the 2-position, as would be expected from the elucidated ^{13}C NMR shifts of the phenothiazine scaffold shown in Fig. 7. Generally, the ^{13}C NMR shift of a carbon atom can be used to estimate the electron density at this atom, because high electron density produces a shielding effect shifting the ^{13}C chemical shift upfield (to lower ppm values). Here the 2-position has a shift of 127.6 ppm, while the 3-position has 122.3 ppm, meaning the 3-position has the higher electron density.

Table 2
Photovoltaic performance of dyes **AFB-3, 20, 22** to **29** under 1 sun AM 1.5G illumination, and from IPCE measurements. All devices were fabricated with 5 mM CDCA in the staining solution.

Dye	Geometry	π-spacer	IPCE J_{SC} (mA cm^{-2})[a]	J_{SC} (mA cm^{-2})	V_{OC} (V)	FF	PCE (%)
AFB-3	3,7-*p*	Ph	7.83	7.65 ± 0.09	807 ± 7	0.71 ± 0.01	4.37 ± 0.10
AFB-9	3,7	Thio	10.43	10.20 ± 0.20	775 ± 8	0.75 ± 0.00	5.82 ± 0.06
AFB-20[b]	3	Thio	8.40	9.13 ± 0.20	778 ± 7	0.76 ± 0.01	5.34 ± 0.11
AFB-22	3	Ph	7.50	7.11 ± 0.16	785 ± 15	0.74 ± 0.02	4.06 ± 0.26
AFB-23[b]	2	Thio	6.34	6.57 ± 0.01	721 ± 8	0.75 ± 0.01	3.48 ± 0.01
AFB-24	2	Ph	4.21	4.17 ± 0.08	753 ± 19	0.74 ± 0.02	2.27 ± 0.03
AFB-25	2,7	Thio	7.48	8.10 ± 0.21	747 ± 4	0.72 ± 0.04	4.27 ± 0.09
AFB-26	2,7	Ph	6.36	6.08 ± 0.14	781 ± 5	0.74 ± 0.01	3.43 ± 0.16
AFB-27	3,8	Thio	9.85	10.11 ± 0.14	774 ± 3	0.75 ± 0.00	5.78 ± 0.09
AFB-28	3,8	Ph	7.89	8.01 ± 0.23	796 ± 16	0.75 ± 0.00	4.67 ± 0.18
AFB-29	3,7-*m*	Ph	2.45	1.95 ± 0.17	713 ± 18	0.78 ± 0.00	1.06 ± 0.10
N719[c]	–	–	–	13.22	784	0.76	7.92

[a] Obtained by integration of the IPCE spectrum over the 1 sun AM 1.5 G spectrum.
[b] Average values of two cells.
[c] Best device. Staining solution of **N719** utilized a solvent mixture of tert-butanol and acetonitrile (1:1, v/v), while staining time and concentration were the same as for the AFB dyes.

3. Conclusion

A total of eleven sensitizers from five phenothiazine geometries have been synthesized and evaluated in dye-sensitized solar cells, with three of the geometries (2, 2,7 and 3,8) being completely novel geometries. The photovoltaic performance of the five geometries for both the thiophene and phenyl π-spacers was in ascending order: 2 < 2,7 < 3 < 3,7 ≈ 3,8. We also established the position of the anchoring group should unquestionably be the 3-position, as is the case for all phenothiazine sensitizers published to date. The most efficient device was sensitized with **AFB-27** from the 3,8 geometry with a *para*-methoxyphenyl auxiliary donor and thiophene π-spacer, delivering a PCE of 5.88% (J_{SC} = 10.28 mA cm^{-2}, V_{OC} = 773 mV, FF = 0.75). The overall performances of the conventional 3,7 and novel 3,8 geometries were near identical, despite the 3,8 geometry displaying a 10% higher dye loading without additives. Consequently, the more linear 3,8 geometry upon optimization has the potential to outperform the bent 3,7 geometry by producing denser dye monolayers, yielding higher short-circuit currents. We hope this study will help the phenothiazine dye class to grow in new directions, yielding higher performing and more versatile phenothiazine sensitizers in the future.

4. Experimental

4.1. Synthesis

A detailed description of the synthesis and characterization of dyes and intermediates is given in the ESI.

4.2. Device fabrication

The photoanodes were fabricated starting from FTO glass (NSG10, Nippon Sheet Glass). It was cleaned in Deconex 21 solution in an ultrasonic bath for 45 min, and then rinsed with deionized water and ethanol. The FTO was further cleaned in a UV/O_3 cleaner for 15 min. A dense blocking layer of TiO_2 was deposited by immersion of the FTO glass slides twice in an aqueous $TiCl_4$ solution at 70 °C for 45 min followed by rinsing with deionized water and ethanol. Screen printing deposited the mesoporous TiO_2 pastes (54T mesh, 2 layers of 18NR-T and 1 layer of WER2-O) with heating to 125 °C for 5 min after each print. Sintering of the TiO_2 was performed on a programmable hotplate following the temperature profile of 125, 250, 375, 450 and 500 °C for 5, 5, 5, 15 and 15 min with ramping times of 5 min between each step. A final $TiCl_4$ post treatment was performed under the same conditions as for the blocking layer, but only once and for 30 min. Sintering at

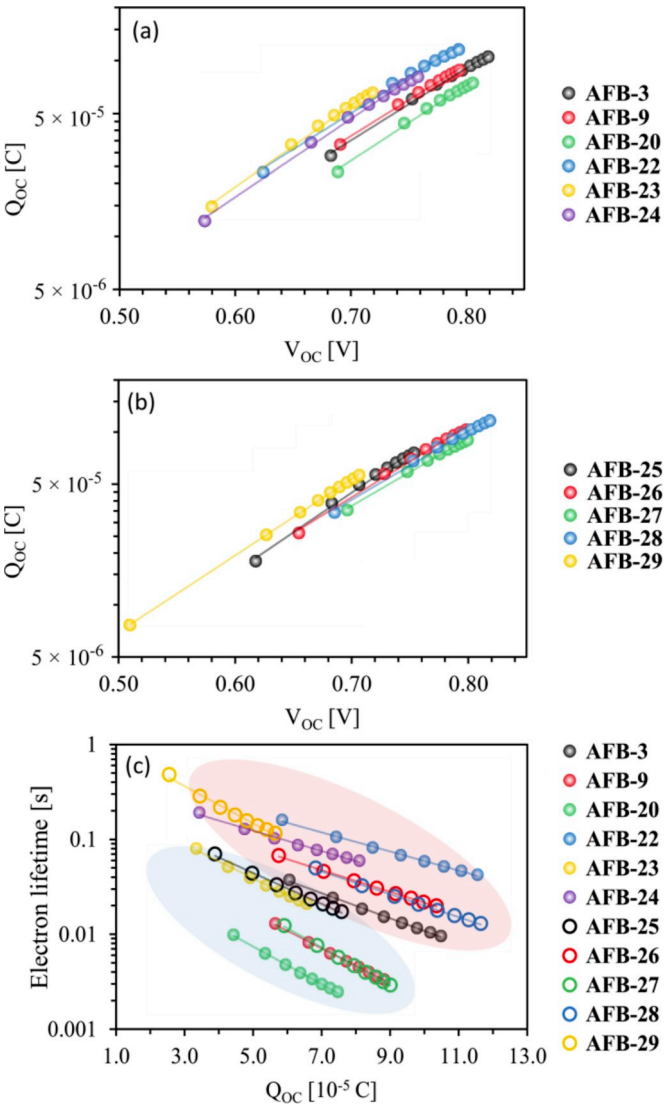

Fig. 6. (a–b) Charge extraction (Q_{OC}) curves for all sensitizers measured at different light intensities, plotted against V_{OC}. (c) Electron lifetime measurements of all dyes, corrected for conduction band shift and plotted against charge extraction values for the same potentials. Sensitizers with thiophene π-spacers are circled in the blue oval while the phenyl π-spacer sensitizers are circled in red. (For interpretation of the references to color in this figure legend, the reader is referred to the Web version of this article.)

Table 3
Dye loading measurements of **AFB-9** and **AFB-27**, without addition of CDCA. Desorption by immersion in a 40 mM solution of TBAOH in stabilized THF, averages of two electrodes.

Dye	Geometry	Dye loading (10^{-7} mol cm^{-2})
AFB-9	3,7	3.95 ± 0.04
AFB-27	3,8	4.34 ± 0.05

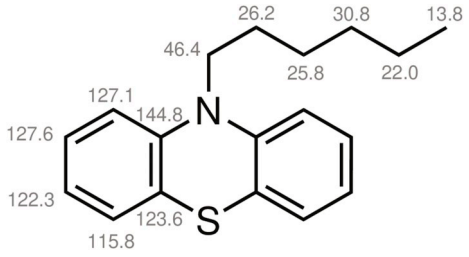

Fig. 7. ^{13}C NMR shifts for 10-hexyl-10*H*-phenothiazine.

500 °C for 45 min on a hotplate was the last step in preparing the photoanodes.

The counter electrodes were prepared from TEC10 FTO glass, holes were drilled with a diamond drill bit under water before the glass slides were cleaned in Hellmanex solution, deionized water, ethanol and acetone, each for 15 min with sonication. The catalytic platinum layer was deposited by drop casting (5 μL/cm^2) a H_2PtCl_6 solution (10 mM in 2-propanol) followed by heating from a hot air gun at 400 °C for 15 min.

Staining of the photoanodes was done in 0.5 mM solutions of the sensitizers with a 10-fold molar excess of chenodeoxycholic acid in a mixture of THF/acetonitrile (57:43, v/v) for 20 h. N719 was stained from a mixture of *tert*-butanol/acetonitrile (1:1, v/v). The stained electrodes were rinsed in acetonitrile for 2 min and air-dried. The solar cells were assembled in a sandwich construction by melting a 25 μm Surlyn gasket between the photoanode and the counter electrode, and filling the cell with A6141 electrolyte by vacuum backfilling. The composition of the A6141 electrolyte was 0.60 M 1-butyl-3-methylimidazolium iodide, 0.03 M I_2, 0.10 M guanidinium thiocyanate and 0.50 M tert-butylpyridine in a mixture of acetonitrile and valeronitrile (85:15, v/v) [41]. Ultrasonic soldering was used to increase the conductivity of the contact points of the electrodes.

4.3. Device characterization

J-V characteristics were measured with a Keithley 2400 under 100 mW/cm^2 illumination from a solar simulator (450 W, Oriel). The devices were masked with a 0.16 cm^2 circular black metal mask. Incident photon-to-current conversion efficiency measurements (IPCE) were recorded on an Arkeo-Ariadne (Cicci Research s.r.l) with a 300 W Xenon lamp. A Dyenamo Toolbox was used for the electron lifetime and charge extraction measurements.

Acknowledgements

The support from the Research Council of Norway to the Norwegian Micro- and Nano-Fabrication Facility, NorFab (project number 245963/F50) and the Norwegian NMR Platform (project number 226244/F50) is highly appreciated.

Appendix A. Supplementary data

Supplementary data to this article can be found online at https://doi.org/10.1016/j.dyepig.2019.05.007.

References

[1] O'Regan B, Grätzel M. Nature 1991;353:737–40.
[2] Freitag M, Teuscher J, Saygili Y, Zhang X, Giordano F, Liska P, Hua J, Zakeeruddin SM, Moser J-E, Grätzel M, Hagfeldt A. Nat Photon 2017;11:372–8.
[3] Joly D, Pelleja L, Narbey S, Oswald F, Meyer T, Kervella Y, Maldivi P, Clifford JN, Palomares E, Demadrille R. Energy Environ Sci 2015;8:2010–8.
[4] Raj A, Steingart D. J Electrochem Soc 2018;165:B3130–6.
[5] Freitag M, Daniel Q, Pazoki M, Sveinbjörnsson K, Zhang J, Sun L, Hagfeldt A, Boschloo G. Energy Environ Sci 2015;8:2634–7.
[6] Freitag M, Giordano F, Yang W, Pazoki M, Hao Y, Zietz B, Grätzel M, Hagfeldt A, Boschloo G. J Phys Chem C 2016;120:9595–603.
[7] Hao Y, Yang W, Zhang L, Jiang R, Mijangos E, Saygili Y, Hammarström L, Hagfeldt A, Boschloo G. Nat Commun 2016;7:13934.
[8] Yum J-H, Baranoff E, Kessler F, Moehl T, Ahmad S, Bessho T, Marchioro A, Ghadiri E, Moser J-E, Yi C, Nazeeruddin MK, Grätzel M. Nat Commun 2012;3:631.
[9] Kakiage K, Aoyama Y, Yano T, Oya K, Fujisawa J-i, Hanaya M. Chem Commun 2015;51:15894–7.
[10] Higashino T, Imahori H. Dalton Trans 2015;44:448–63.
[11] Mathew S, Yella A, Gao P, Humphry-Baker R, Curchod BFE, Ashari-Astani N, Tavernelli I, Rothlisberger U, Nazeeruddin K, Grätzel M. Nat Chem 2014;6:242–7.
[12] Ahmad S, Guillen E, Kavan L, Grätzel M, Nazeeruddin MK. Energy Environ Sci 2013;6:3439–66.
[13] Mishra A, Fischer MK, Baüerle P. Angew Chem Int Ed 2009;48:2474–99.
[14] Sheibani E, Zhang L, Liu P, Xu B, Mijangos E, Boschloo G, Hagfeldt A, Hammarström L, Kloo L, Tian H. RSC Adv 2016;6:18165–77.
[15] Tian H, Yang X, Chen R, Pan Y, Li L, Hagfeldt A, Sun L. Chem Commun 2007:3741–3.
[16] Tian H, Yang X, Cong J, Chen R, Liu J, Hao Y, Hagfeldt A, Sun L. Chem Commun 2009:6288–90.
[17] Lin RY-Y, Wu F-L, Li C-T, Chen P-Y, Ho K-C, Lin JT. ChemSusChem 2015;8:2503–13.
[18] Luo J-S, Wan Z-Q, Jia C-Y. Chin Chem Lett 2016;27:1304–18.
[19] Huang Z-S, Meier H, Cao D. J Mater Chem C 2016;4:2404–26.
[20] Katsuhiko O, Tomoya Y, Masaaki T. Chem Lett 2010;39:864–6.
[21] Hart AS, K.C CB, Subbaiyan NK, Karr PA, D'Souza F. ACS Appl Mater Interfaces 2012;4:5813–20.
[22] Wan Z, Jia C, Duan Y, Zhou L, Lin Y, Shi Y. J Mater Chem 2012;22:25140–7.
[23] Chiykowski VA, Lam B, Du C, Berlinguette CP. Chem Commun 2017;53:2367–70.
[24] Chiykowski VA, Lam B, Du C, Berlinguette CP. Chem Commun 2017;53:2547–50.
[25] Lu Y, Song H, Li X, Ågren H, Liu Q, Zhang J, Zhang X, Xie Y. ACS Appl Mater Interfaces 2019;11:5046–54.
[26] Kumar R, Sudhakar V, Prakash K, Krishnamoorthy K, Sankar M. ACS Appl Mater Interfaces 2018;1:2793–801.
[27] Yang G, Tang Y, Li X, Ågren H, Xie Y. ACS Appl Mater Interfaces 2017;9:36875–85.
[28] Krishna NV, Krishna JVS, Singh SP, Giribabu L, Han L, Bedja I, Gupta RK, Islam A. J Phys Chem C 2017;121:6464–77.
[29] Marszalek M, Nagane S, Ichake A, Humphry-Baker R, Paul V, Zakeeruddin SM, Grätzel M. J Mater Chem 2012;22:889–94.
[30] Kim SH, Sakong C, Chang JB, Kim B, Ko MJ, Kim DH, Hong KS, Kim JP. Dyes Pigments 2013;97:262–71.
[31] Buene AF, Uggerud N, Economopoulos SP, Gautun OR, Hoff BH. Dyes Pigments 2018;151:263–71.
[32] Buene AF, Ose EE, Zakariassen AG, Hagfeldt A, Hoff BH. J Mater Chem A 2019;7:7581–90.
[33] Chen J, Zhang Y, Yang L, Zhang X, Liu J, Li L, Zhang H. Tetrahedron 2007;63:4266–70.
[34] Wei H, Shen J, Liu Y, Huang T, Zhang Q, Zhao J, Zhao X. Dyes Pigments 2018;149:789–95.
[35] Yang YS, Kim HD, Ryu J-H, Kim KK, Park SS, Ahn K-S, Kim JH. Synth Met 2011;161:850–5.
[36] Marinado T, Nonomura K, Nissfolk J, Karlsson MK, Hagberg DP, Sun L, Mori S, Hagfeldt A. Langmuir 2010;26:2592–8.
[37] Wang S, Guo J, He L, Wang H, Zhao J, Lu C. Synth Met 2013;168:1–8.
[38] Hagfeldt A, Grätzel M. Chem Rev 1995;95:49–68.
[39] Teuscher J, Marchioro A, Andrès J, Roch LM, Xu M, Zakeeruddin SM, Wang P, Grätzel M, Moser J-E. J Phys Chem C 2014;118:17108–15.
[40] Baumann A, Cheema H, Sabuj MA, McNamara LE, Zhang Y, Peddapuram A, Nguyen ST, Watkins DL, Hammer NI, Rai N, Delcamp JH. Phys Chem Chem Phys 2018;20:17859–70.
[41] Nazeeruddin MK, De Angelis F, Fantacci S, Selloni A, Viscardi G, Liska P, Ito S, Takeru B, Grätzel M. JACS 2005;127:16835–47.